

Ultralow and Anisotropic Thermal Conductivity in Semiconductor As₂Se₃

Robert L. González-Romero,^{a,b} Alex Antonelli,^b Anderson S. Chaves,^b and Juan J. Meléndez^{*c,d}

Abstract

An ultralow lattice thermal conductivity of 0.14 W · m⁻¹ · K⁻¹ along the \vec{b} axis of As₂Se₃ single crystals was obtained at 300 K by first-principles calculations involving the density functional theory and the resolution of the Boltzmann transport equation. The origin of this ultralow thermal conductivity arises from a cascade-like fall of the optical modes coupled to the avoided-crossing of these and transverse acoustic modes. These results, whose validity has been addressed by comparison with SnSe, for which excellent agreement between the theoretical predictions and the experiments is achieved, point out that As₂Se₃ could exhibit improved thermoelectric properties.

1 Introduction

Semiconductor materials have played a crucial role in the development of the modern societies due to their conducting properties. Lately, insofar the electronic devices are becoming smaller, their thermal and thermoelectric performances are becoming more and more relevant. In particular, semiconductors with low thermal conductivities are indispensable to design and develop high-efficiency thermoelectric devices¹⁻³. As a general rule, at room temperature or higher, the lattice vibrations (phonons) drive most of the heat, and this transport is ruled mostly by the phonon-phonon scattering processes resulting from the anharmonicity of the interatomic potential. At low temperatures (or in nanostructured samples), extrinsic scattering by point defects, isotopes or grain boundaries become relevant as well⁴.

It seems clear then that an accurate description and comprehension of the several phonon scattering processes is required to understand how material properties relate to the lattice thermal conductivity κ_L . In addition, understanding phonon-phonon scattering paves the way to design strategies to tailor thermal transport. In this respect, the predictive first-principles calculations based upon solutions of the Boltzmann transport equation (BTE) for phonons⁵ constitute a significant progress. These calculations allow one to calculate κ_L without the need of adjustable parameters⁶⁻⁸. Their reliability has been demonstrated by using them in many distinct systems such as skutterudites⁹⁻¹², clathrates¹³, chalcogenides¹⁴⁻¹⁷ and other systems¹⁸⁻²⁰. An additional advantage of the first-principles calculations based upon BTE is that they shed light about heat conduction through intermediate magnitudes such as the scattering rates or the three-phonon scattering phase spaces for phonons, which are difficult to access in experiments.

2 Theoretical framework

Within the BTE formalism under the relaxation time approximation (RTA) and the assumption of a uniform temperature gradient^{6,7,21,22}, the lattice thermal conductivity at a given temperature may be calculated as a sum of contributions over all the phonon modes λ with wave vector \vec{q} ⁸:

$$\kappa_L \equiv \kappa_L^{\alpha\alpha} = \frac{1}{NV} \sum_{\lambda} \frac{\partial f}{\partial T} (\hbar\omega_{\lambda}) v_{\lambda}^{\alpha} v_{\lambda}^{\alpha} \tau_{\lambda}, \quad (1)$$

where N is the number of uniformly spaced \vec{q} points within the first Brillouin zone (ZB), V is the volume of the unit cell, f is the Bose-Einstein distribution function, depending on the phonon frequency ω_{λ} , v_{λ}^{α} is the phonon velocity along the α direction and τ_{λ} is the phonon lifetime.

Solving BTE requires knowing the harmonic interatomic force constants (h-IFC), as input parameters to calculate the phonons frequencies and velocities, as well as the phonon lifetimes τ_{λ} . For bulk materials, the inverse of τ_{λ} equals the total scattering velocity, which is the sum of the isotropic ($1/\tau^{iso}$) and the anharmonic scattering rates ($1/\tau^{anh}$). In general, $1/\tau^{iso}$ is lower than $1/\tau^{anh}$, so that only the later is usually considered in calculations of thermal conductivity (see ESI†, Fig. S1, for details). On the other hand, $1/\tau^{anh}$ may be calculated as the sum of three-phonon transition probabilities $\Gamma_{\lambda\lambda'\lambda''}^{\pm}$, defined as^{6-8,14}:

$$\Gamma_{\lambda\lambda'\lambda''}^{\pm} = \frac{\pi\hbar}{8N} \left\{ \begin{array}{l} 2(f_{\lambda'} - f_{\lambda''}) \\ f_{\lambda'} + f_{\lambda''} + 1 \end{array} \right\} \frac{\delta(\omega_{\lambda} \pm \omega_{\lambda'} - \omega_{\lambda''})}{\omega_{\lambda} \omega_{\lambda'} \omega_{\lambda''}} |V_{\lambda\lambda'\lambda''}^{\pm}|^2, \quad (2)$$

where the upper (lower) row within curly brackets with the “+” (“-”) sign corresponds to the phonon absorption (emission) processes. In Eq. (2), δ holds for the Dirac delta distribution and $V_{\lambda\lambda'\lambda''}^{\pm}$ are the scattering matrix elements, which are obtained from the normalized eigenvectors for the three phonons involved in the scattering process and the corresponding anharmonic interatomic force constants (a-IFCs)⁸. Both the second-order h-IFC and the third-order a-IFC can be calculated within a real-space finite-difference supercell approach within the density functional theory (DFT)⁸. Another magnitude that sheds light about phonon scattering processes is the three-phonon scattering phase space W^{\pm} (the “+” and “-” signs corresponding to the absorption and emission processes, respectively). W^{\pm} accounts for the contribution of the harmonic phonon frequencies to the anharmonic scattering rates and is defined as the sum of frequency-containing factors in the expression of three-phonon transition probabilities, Eq. (2)⁹:

$$W_{\lambda}^{\pm} = \frac{1}{2N} \sum_{\lambda',\lambda''} \left\{ \begin{array}{l} 2(f_{\lambda'} - f_{\lambda''}) \\ f_{\lambda'} + f_{\lambda''} + 1 \end{array} \right\} \frac{\delta(\omega_{\lambda} \pm \omega_{\lambda'} - \omega_{\lambda''})}{\omega_{\lambda} \omega_{\lambda'} \omega_{\lambda''}} \quad (3)$$

^{0a} Dpto. de Sistemas Físicos, Químicos y Naturales. Universidad Pablo de Olavide, Sevilla, Spain.

^{0b} Instituto de Física Gleb Wataghin, Universidade Estadual do Campinas, Campinas, Brazil.

^{0c} Dpto. de Física, Universidad de Extremadura, Avda. de Elvas, s/n, 06007 Badajoz, Spain. Fax: +34 924 28 96 51; Tel: +34 924 28 96 51, E-mail: melendez@unex.es

^{0d} Instituto de Computación Científica Avanzada de Extremadura (ICCAE), Badajoz, Spain.

In this work, we have used a first-principles BTE approach to calculate κ_L of the As_2Se_3 system, which was widely studied during the 70's because of its excellent optical and electronic properties²³⁻²⁷. As_2Se_3 is a semiconductor with relatively complex structure (monoclinic, space group Nr. 14, $P2_1/n$). Its unit cell contains 20 atoms disposed in a stacked bilayer configuration (see ESI†, Fig. S2). It has an indirect gap ranging between 1.3 and 1.5 eV^{23,27}, and its effective masses are low²³. A peculiarity of As_2Se_3 is that it exhibits relatively flat electronic bands near the gap, similar to the “pudding mold” bands proposed by Kuroki and Arita²⁸. All these features make one wonder whether As_2Se_3 could be a good candidate material for potential thermoelectric applications. The preliminary step for this inquiry is to evaluate the lattice thermal properties of this system, which have not been studied before to the best of our knowledge.

3 Computational methods

DFT first-principles calculations^{29,30} have been performed using the projector augmented wave (PAW) method³¹ as implemented in the Vienna ab initio simulation package (VASP)³². The Perdew-Burke-Ernzerhof functional for the generalized-gradient-approximation (GGA) was used to describe the exchange-correlation functional³³. Van der Waals correction modeled by the DFT-D method by Grimme *et al.*³⁴ were explicitly included, as they yield optimized results in these types of structures¹⁷. The kinetic energy cutoff of wave functions was set to 650 eV, and a Monkhorst-Pack k -mesh of $4 \times 6 \times 12$ was used to sample the first Brillouin zone (BZ) for integrations in the reciprocal space³⁵. A force less than 10^{-5} eV/Å and a total change in energy less than 10^{-7} eV were selected as convergence criteria for the structural optimization.

The first-principles lattice thermal conductivity κ_L was calculated by solving BTE for phonons. The IFCs were calculated within a real-space supercell approach by using the Phonopy package³⁶ for the two-order h-IFC and the ShengBTE package⁸ for the third-order a-IFC. The h-IFC were calculated using a $2 \times 2 \times 2$ supercell with a $2 \times 3 \times 6$ k -mesh, while a $2 \times 2 \times 3$ supercell was used for the third-order a-IFC; the Γ point only was used to sample BZ in this case, and a cutoff of 5.6 Å for the interaction range was employed.

4 Results and discussion

After the structural relaxation, As_2Se_3 exhibited a monoclinic unit cell with lattice parameters $a = 12.20(12.08)$ Å, $b = 10.04(9.90)$ Å, $c = 4.27(4.28)$ Å and $\beta = 90.51(90.46)^\circ$, in very good agreement with experimental results taken from the literature (into brackets)^{23,37}. The structural details are reported within the ESI†, Fig. S2.

Fig. 1 shows the lattice thermal conductivity κ_L as a function of temperature for As_2Se_3 . For comparison purposes, Fig. 1 includes previous results obtained using the same methodology for SnSe¹⁷. This figure reveals a strong anisotropy and an astonishing small value for the lattice thermal conductivity along the \vec{b} axis, which is roughly one order of magnitude lower than that within the ac plane: at room temperature, the values of κ_L (in $\text{W} \cdot \text{m}^{-1} \cdot \text{K}^{-1}$) along the \vec{a} , \vec{b} and \vec{c} axes are 1.34, 0.14 and 0.97, respectively. Compared to values currently reported in the literature for thermoelectric materials^{3,38}, the κ_L value along \vec{b} is even lower than those observed in nanostructures and all-scale hierarchical architecture of PbTe-based thermoelectrics³⁹. Besides, κ_L varies with temperature as T^{-1} , which is the characteristic law for intrinsic three-phonon scattering. Unfortunately, there are not experimental measurements of thermal conductivity for As_2Se_3 single crystals, to our knowledge. The validity of our results should be based on the many papers proving the reliability of our methodology^{8,12,15}. An additional proof comes from the comparison between our results and those by Vaney *et al.*⁴⁰ for α - As_2Te_3 polycrystals (see ESI†, Fig. S3), which shows a very good agreement.

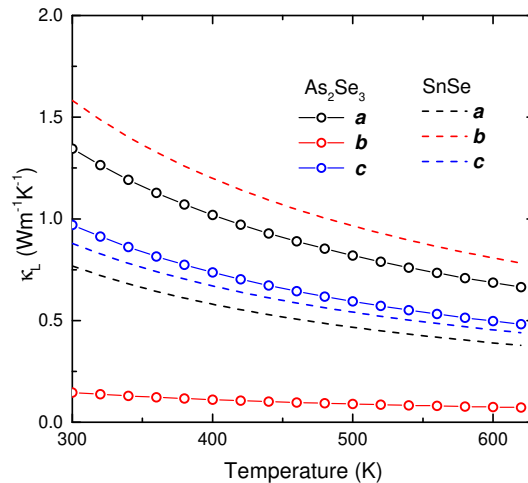


Figure 1 Lattice thermal conductivity of As_2Se_3 along the unit cell axes as functions of the temperature. Data for SnSe are included for comparison.

As we mentioned in the introduction, the deep comprehension of the thermal conductivity phenomena in semiconductors requires a correct description of their vibrational behavior. Fig. 2a plots the phonon spectrum of As_2Se_3 along high-symmetry directions of the BZ. This spectrum is moderately complex, with a two-part configuration containing a wide gap between 140 - 180 cm^{-1} , approximately, and four narrower gaps within the 180 - 275 cm^{-1} range. A remarkable feature of this spectrum is the severe mixture of low-lying optical modes (blue lines in Fig. 2a) and acoustic modes (red lines). This cascade-like fall of the optical modes, as well as the avoided-crossing behavior of the transverse acoustic and optical modes around Γ , appears in a number of solids with very low thermal

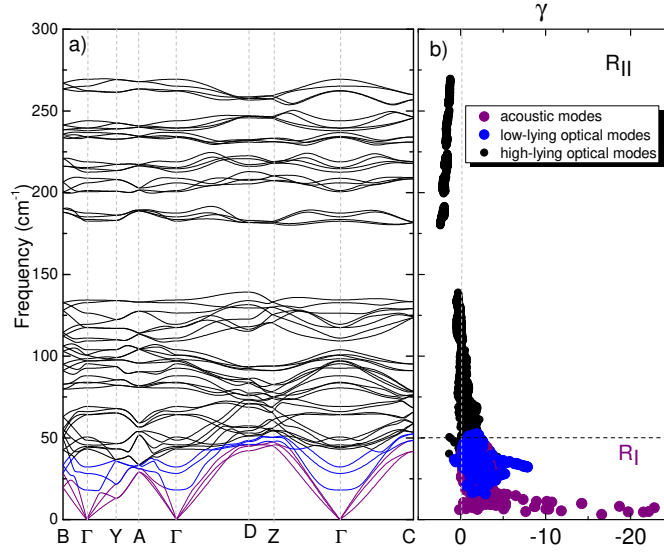


Figure 2 a) Phonon spectrum for As_2Se_3 along high-symmetry directions of BZ. b) Variation of the Grüneisen parameter with the phonon frequency.

conductivities^{16,41–43}. For this particular case, in addition, the low-lying optical branches exhibit frequencies of 18 (21.5), 28 (27) and 32 (32.5) cm^{-1} at Γ , in very good agreement with Raman spectroscopy results reported by Zallen and Slade (into brackets)⁴⁴.

In turn, the low frequency of the optical phonons results in a softening of the acoustic branches, which yields low sound velocities and, therefore, low Debye temperatures θ_D . From the phonon spectrum in Fig. 2a one gets $\theta_D = 128$ K, $\theta_D = 116$ K and $\theta_D = 181$ K along the \vec{a} , \vec{b} and \vec{c} crystal axes, respectively, which correlates well with the strong anisotropy of the system. According to the Slack theory⁴⁵, low Debye temperatures are indicative of low thermal conductivities. The reason is that low θ_D values are related to low group velocities and frequencies for acoustic phonons, which yields higher phonon populations and, therefore, higher phonon scattering rates¹⁹.

The phonon scattering rate depends basically upon two factors¹⁹: the strength of each scattering channel, which depends on the anharmonicity and is described by the Grüneisen parameter γ , and the number of channels available for the phonons to be scattered; the later are characterized by the phase spaces for three-phonon processes (W^\pm). Fig 2b shows the Grüneisen parameter of As_2Se_3 as a function of frequency. For clarity, we have divided the plot into two regions, namely R_I , corresponding to acoustic and low-lying optical phonons, and R_{II} , corresponding to optical modes with frequency above 50 cm^{-1} . The phonon softening results in an increase of the anharmonicity of the system, and γ reaches high absolute values. Hence, it is expected that the system exhibits low thermal conductivity, as has been observed in other systems^{14,43}. In addition, according to Fu *et al.*¹², negative γ values for the low-lying optical branches imply that these modes may be softened further by compression and, therefore, may exhibit a more severe overlap with the acoustic branches, as well as wider W^\pm values. In other words, it is expectable that κ_L decreases even more at high pressures.

In Eq. (1) we show that the phonon lifetimes are directly related with reduce κ_L . At temperatures above θ_D , they are ruled by three-phonon anharmonic scattering processes¹². Fig. 3 plots the anharmonic scattering rates $1/\tau^{anh}$, where τ^{anh} is the mean anharmonic lifetime for phonons, calculated at 300 K. For comparison purposes, results for SnSe are included as well¹⁷. The inset in Fig. 3 shows the normalized cumulative lattice thermal conductivity vs. the phonon frequency for As_2Se_3 and SnSe.

In both systems, the anharmonic scattering rates for acoustic and optical phonons with frequencies below approximately 50 cm^{-1} are between two (As_2Se_3 case) and three (SnSe case) orders of magnitude lower than those with higher frequencies, for each material. For As_2Se_3 , the scattering rates for ultralow-frequency phonons are higher than for SnSe; the contribution of the later to κ_L is obviously different, as evidenced by the different slopes in the inset of Fig. 3. In addition, in both systems, roughly 70% of the heat is driven by phonons with frequency below 65 cm^{-1} (shaded region in the inset of Fig. 3). In this same frequency range one observes a split between the scattering rates for both systems; thus, at around 65 cm^{-1} the scattering rates are approximately equal for As_2Se_3 as for SnSe, but at higher frequencies $1/\tau^{anh}$ is smaller for the former. It is worthwhile to note that the contribution to the heat current by the optical branches with frequencies above the gap is different in both cases. From the inset in Fig. 3 one observes that the contribution of these modes is around 24% for SnSe, whereas it is barely of the 7% for As_2Se_3 .

According to Eq. (2), the anharmonic scattering rates are proportional to the squares of the a-IFC. Therefore, the anharmonic interatomic force constants for both systems are approximately comparable, at least for frequencies above about 30 cm^{-1} . The question arises as to understand the low conductivity of As_2Se_3 along the \vec{b} axis, that is, perpendicularly to the structural bilayers. To clarify this issue, Fig. 4 plots the three-phonon scattering phase spaces, W^\pm . Essentially, these quantities represent the number of scattering channels for three-phonon processes available to all the modes, and vary inversely with κ_L ⁴⁶. Thus, the W^\pm values provide insights about the effect of the phonon frequencies on the anharmonic scattering rate via their contribution to the three-phonon scattering matrix elements¹².

Fig. 4 indicates that the scattering phase spaces are significantly higher in As_2Se_3 , especially at low vibrational frequencies, whereas both As_2Se_3 and SnSe exhibit comparable values of W^\pm for optical modes with frequencies above their respective gaps. At low frequencies, both absorption and emission are equally probable in As_2Se_3 , as it was expectable. However, there are marked differences

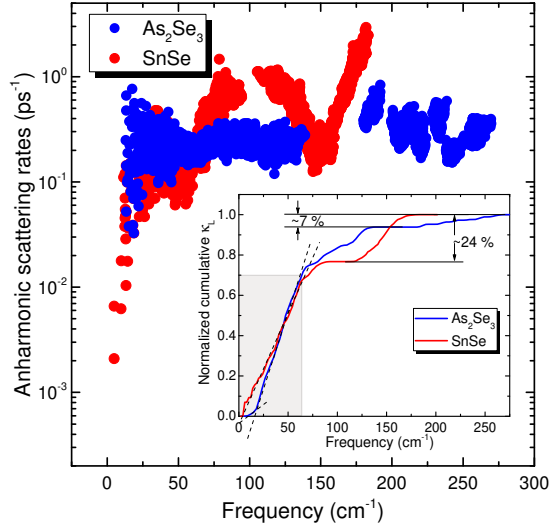


Figure 3 Anharmonic scattering rates vs. frequency for As_2Se_3 and SnSe . The inset shows the cumulative lattice conductivity as a function of the frequency for both systems.

between 50 and 150 cm^{-1} , as well as at frequencies above about 220 cm^{-1} , where absorption predominates. The widening of W^\pm for As_2Se_3 results from the shape of the phonon spectrum, where the low-lying optical branches overlap the acoustic ones (see Fig. 2a). As a consequence, the anharmonicity of the system as well as the phase spaces increase, and this facilitates phonon scattering.

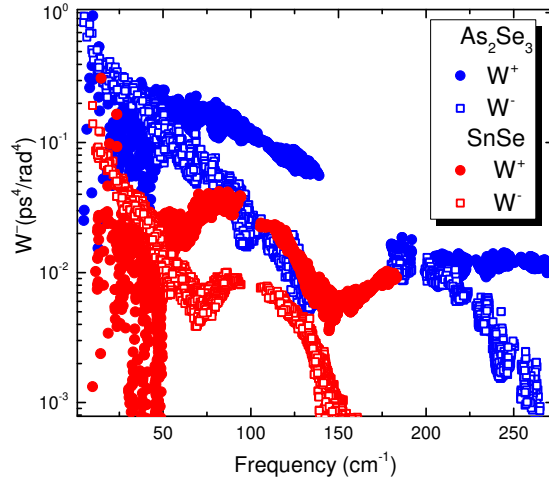


Figure 4 Absorption and emission three-phonon scattering phase spaces for As_2Se_3 and SnSe as functions of the frequency.

The anisotropy and low values of lattice thermal conductivity in As_2Se_3 can be understood then from the discussion by Nielsen *et al.*⁴⁶. These authors argue that chalcogenides such as SnSe , among other similar systems, have electrons forming “lone pairs” in s^2 orbitals ($\text{Sn-}5s^2$ for SnSe or $\text{As-}4s^2$ for As_2Se_3) that do not contribute to the chemical bonds but interact with the bonding orbitals within the lattice, and this fact is responsible for the anharmonicity in the system. Besides, the low thermal conductivity of both systems in the direction perpendicular to the layers of their respective structures (along \vec{b} in SnSe or along \vec{a} in As_2Se_3) is related to the low-lying optical modes. These modes are in turn responsible for the important scattering of the acoustic phonons, which takes place because at those low frequencies the layers move rigidly, as schematized in Fig. 5. This causes the effective masses of the acoustic modes to be much higher than that for modes in which the atoms move individually (see ESI†, animated figures). Since the As_2Se_3 unit cell is more complex and has more atoms, the vibration frequencies of their optical modes are lower than those for SnSe .

5 Conclusions

In conclusion, the first-principles calculations reported in this work suggest that As_2Se_3 is a promising candidate for thermoelectric applications which deserves an experimental exploration. Indeed, its κ_L values are extremely low, of the order of 0.14 $\text{W}\cdot\text{m}^{-1}\cdot\text{K}^{-1}$ at room temperature. This low thermal conductivity is due, on one hand, to the strong anharmonicity of the system and, on the other hand, to its high scattering phase space values.

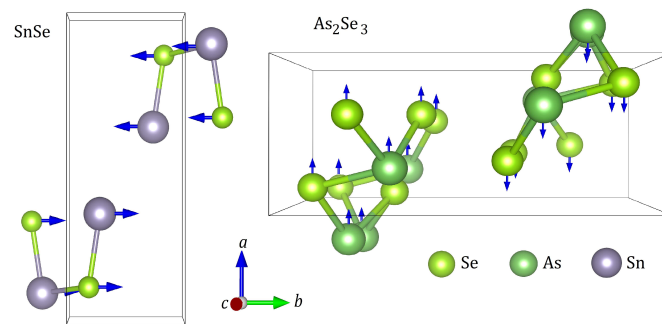


Figure 5 Schematic representation of the low-lying optical modes causing the rigid vibration of the atomic layers along the \vec{b} (SnSe, left figure) and \vec{a} (As_2Se_3 , upper right figure) axes.

6 Acknowledgements

We gratefully acknowledge support from the Brazilian agencies CNPq, CAPES, and the Center for Computational Engineering and Science-Fapesp/Cepid #2013/08293-7 and FAPESP under Grant #2013/14065-7. Financial support by the Junta of Extremadura in Spain through Grants GR15105 and IB16013 is acknowledged as well. The calculations were performed at CCJDR-IFGW-UNICAMP and at CENAPAD-SP in Brazil.

References

- [1] J. Yang, L. Xi, W. Qiu, L. Wu, X. Shi, L. Chen, J. Yang, W. Zhang, C. Uher and D. J. Singh, *Npj Comput. Mater.*, 2016, **2**, 15015.
- [2] W. He, G. Zhang, X. Zhang, J. Ji, G. Li and X. Zhao, *Appl. Energ.*, 2015, **143**, 1 – 25.
- [3] L.-D. Zhao, V. P. Dravid and M. G. Kanatzidis, *Energy Environ. Sci.*, 2014, **7**, 251–268.
- [4] J. M. Ziman, *Electrons and phonons: the theory of transport phenomena in solids*, Oxford University Press, 1960.
- [5] R. E. Peierls, *Quantum theory of solids*, Oxford University Press, 2001.
- [6] A. Ward, D. A. Broido, D. A. Stewart and G. Deinzer, *Phys. Rev. B*, 2009, **80**, 125203.
- [7] D. A. Broido, M. Malorny, G. Birner, N. Mingo and D. A. Stewart, *Appl. Phys. Lett.*, 2007, **91**, 231922.
- [8] W. Li, J. Carrete, N. A. Katcho and N. Mingo, *Comput. Phys. Commun.*, 2014, **185**, 1747–1758.
- [9] W. Li and N. Mingo, *Phys. Rev. B*, 2014, **90**, 094302.
- [10] W. Li and N. Mingo, *Phys. Rev. B*, 2014, **89**, 184304.
- [11] R. Guo, X. Wang, Y. Kuang and B. Huang, *Phys. Rev. B*, 2015, **92**, 115202.
- [12] Y. Fu, D. J. Singh, W. Li and L. Zhang, *Phys. Rev. B*, 2016, **94**, 075122.
- [13] T. Tadano, Y. Gohda and S. Tsuneyuki, *Phys. Rev. Lett.*, 2015, **114**, 095501.
- [14] Z. Tian, J. Garg, K. Esfarjani, T. Shiga, J. Shiomi and G. Chen, *Phys. Rev. B*, 2012, **85**, 184303.
- [15] J. Carrete, N. Mingo and S. Curtarolo, *Appl. Phys. Lett.*, 2014, **105**, 101907.
- [16] A. H. Romero, E. K. U. Gross, M. J. Verstraete and O. Hellman, *Phys. Rev. B*, 2015, **91**, 214310.
- [17] R. L. González-Romero, A. Antonelli and J. J. Meléndez, *Phys. Chem. Chem. Phys.*, 2017, **19**, 12804–12815.
- [18] B. Peng, H. Zhang, H. Shao, Y. Xu, X. Zhang and H. Zhu, *Sci. Rep.*, 2016, **6**, 20225.
- [19] B. Peng, H. Zhang, H. Shao, Y. Xu, G. Ni, R. Zhang and H. Zhu, *Phys. Rev. B*, 2016, **94**, 245420.
- [20] S. Mukhopadhyay, L. Lindsay and D. S. Parker, *Phys. Rev. B*, 2016, **93**, 224301.
- [21] L. Lindsay, D. A. Broido and T. L. Reinecke, *Phys. Rev. Lett.*, 2012, **109**, 095901.
- [22] L. Lindsay, D. A. Broido and T. L. Reinecke, *Phys. Rev. B*, 2013, **87**, 165201.
- [23] E. Tarnow, A. Antonelli and J. D. Joannopoulos, *Phys. Rev. B*, 1986, **34**, 4059–4073.

- [24] E. Tarnow, A. Antonelli and J. D. Joannopoulos, *Phys. Rev. B*, 1986, **34**, 8718–8727.
- [25] R. Zallen, R. E. Drews, R. L. Emerald and M. L. Slade, *Phys. Rev. Lett.*, 1971, **26**, 1564–1567.
- [26] V. V. Struzhkin, A. F. Goncharov, R. Caracas, H.-k. Mao and R. J. Hemley, *Phys. Rev. B*, 2008, **77**, 165133.
- [27] Y. Sharma and P. Srivastava, *Comp. Mater. Sci.*, 2012, **53**, 451 – 459.
- [28] K. Kuroki and R. Arita, *J. Phys. Soc. Jpn.*, 2007, **76**, 083707.
- [29] P. Hohenberg and W. Kohn, *Phys. Rev.*, 1964, **136**, B864–B871.
- [30] W. Kohn and L. J. Sham, *Phys. Rev.*, 1965, **140**, A1133–A1138.
- [31] P. E. Blöchl, *Phys. Rev. B*, 1994, **50**, 17953–17979.
- [32] G. Kresse and J. Furthmüller, *Phys. Rev. B*, 1996, **54**, 11169–11186.
- [33] J. P. Perdew, K. Burke and M. Ernzerhof, *Phys. Rev. Lett.*, 1996, **77**, 3865–3868.
- [34] S. Grimme, J. Antony, S. Ehrlich and J. Krieg, *J. Chem. Phys.*, 2010, **132**, 154104.
- [35] H. J. Monkhorst and J. D. Pack, *Phys. Rev. B*, 1976, **13**, 5188–5192.
- [36] A. Togo and I. Tanaka, *Scripta Mater.*, 2015, **108**, 1–5.
- [37] A. C. Stergiou and P. J. Rentzeperis, *Z. Krist.-Cryst. Mater.*, 1985, **173**, 185–192.
- [38] G. J. Snyder and E. S. Toberer, *Nat. Mater.*, 2008, **7**, 105–114.
- [39] K. Biswas, J. He, I. D. Blum, C.-I. Wu, T. P. Hogan, D. N. Seidman, V. P. Dravid and M. G. Kanatzidis, *Nature*, 2012, **489**, 414–418.
- [40] J. B. Vaney, J. Carreaud, G. Delaizir, A. Piarristeguy, A. Pradel, E. Alleno, J. Monnier, E. B. Lopes, A. P. Goncalves, A. Dauscher, C. Candolfi and B. Lenoir, *J. Mater. Chem. C*, 2016, **4**, 2329–2338.
- [41] S. Lee, K. Esfarjani, T. Luo, J. Zhou, Z. Tian and G. Chen, *Sci. Rep.*, 2014, **5**, 3525.
- [42] Y. Luo, J. Wang, Y. Li and J. Wang, *Sci. Rep.*, 2016, **6**, 29801.
- [43] O. Delaire, J. Ma, K. Marty, A. F. May, M. A. McGuire, M.-H. Du, D. J. Singh, A. Podlesnyak, G. Ehlers, M. D. Lumsden and B. C. Sales, *Nat Mater*, 2011, **10**, 614–619.
- [44] R. Zallen and M. Slade, *Phys. Rev. B*, 1974, **9**, 1627–1637.
- [45] D. T. Morelli and G. A. Slack, in *High Lattice Thermal Conductivity Solids*, ed. S. L. Shindé and J. S. Goela, Springer New York, New York, NY, 2006, pp. 37–68.
- [46] M. D. Nielsen, V. Ozolins and J. P. Heremans, *Energy Environ. Sci.*, 2013, **6**, 570–578.